

Measurement of the $W + b$ -jet and $W + c$ -jet differential production cross sections in $p\bar{p}$ collisions at $\sqrt{s} = 1.96$ TeV

V.M. Abazov,³¹ B. Abbott,⁶⁷ B.S. Acharya,²⁵ M. Adams,⁴⁶ T. Adams,⁴⁴ J.P. Agnew,⁴¹ G.D. Alexeev,³¹ G. Alkhazov,³⁵ A. Alton^a,⁵⁶ A. Askew,⁴⁴ S. Atkins,⁵⁴ K. Augsten,⁷ C. Avila,⁵ F. Badaud,¹⁰ L. Bagby,⁴⁵ B. Baldin,⁴⁵ D.V. Bandurin,⁷³ S. Banerjee,²⁵ E. Barberis,⁵⁵ P. Baringer,⁵³ J.F. Bartlett,⁴⁵ U. Bassler,¹⁵ V. Bazterra,⁴⁶ A. Bean,⁵³ M. Begalli,² L. Bellantoni,⁴⁵ S.B. Beri,²³ G. Bernardi,¹⁴ R. Bernhard,¹⁹ I. Bertram,³⁹ M. Besançon,¹⁵ R. Beuselinck,⁴⁰ P.C. Bhat,⁴⁵ S. Bhatia,⁵⁸ V. Bhatnagar,²³ G. Blazey,⁴⁷ S. Blessing,⁴⁴ K. Bloom,⁵⁹ A. Boehnlein,⁴⁵ D. Boline,⁶⁴ E.E. Boos,³³ G. Borissov,³⁹ M. Borysova^l,³⁸ O. Borysov,³⁸ A. Brandt,⁷⁰ O. Brandt,²⁰ R. Brock,⁵⁷ A. Bross,⁴⁵ D. Brown,¹⁴ X.B. Bu,⁴⁵ M. Buehler,⁴⁵ V. Buescher,²¹ V. Bunichev,³³ S. Burdin^b,³⁹ C.P. Buszello,³⁷ E. Camacho-Pérez,²⁸ B.C.K. Casey,⁴⁵ H. Castilla-Valdez,²⁸ S. Caughron,⁵⁷ S. Chakrabarti,⁶⁴ K.M. Chan,⁵¹ A. Chandra,⁷² E. Chapon,¹⁵ G. Chen,⁵³ S.W. Cho,²⁷ S. Choi,²⁷ B. Choudhary,²⁴ S. Cihangir,⁴⁵ D. Claes,⁵⁹ J. Clutter,⁵³ M. Cooke^k,⁴⁵ W.E. Cooper,⁴⁵ M. Corcoran,⁷² F. Couderc,¹⁵ M.-C. Cousinou,¹² D. Cutts,⁶⁹ A. Das,⁴² G. Davies,⁴⁰ S.J. de Jong,^{29,30} E. De La Cruz-Burelo,²⁸ F. Déliot,¹⁵ R. Demina,⁶³ D. Denisov,⁴⁵ S.P. Denisov,³⁴ S. Desai,⁴⁵ C. Deterre^c,⁴¹ K. DeVaughan,⁵⁹ H.T. Diehl,⁴⁵ M. Diesburg,⁴⁵ P.F. Ding,⁴¹ A. Dominguez,⁵⁹ A. Dubey,²⁴ L.V. Dudko,³³ A. Duperrin,¹² S. Dutt,²³ M. Eads,⁴⁷ D. Edmunds,⁵⁷ J. Ellison,⁴³ V.D. Elvira,⁴⁵ Y. Enari,¹⁴ H. Evans,⁴⁹ V.N. Evdokimov,³⁴ A. Fauré,¹⁵ L. Feng,⁴⁷ T. Ferbel,⁶³ F. Fiedler,²¹ F. Filthaut,^{29,30} W. Fisher,⁵⁷ H.E. Fisk,⁴⁵ M. Fortner,⁴⁷ H. Fox,³⁹ S. Fuess,⁴⁵ P.H. Garbincius,⁴⁵ A. Garcia-Bellido,⁶³ J.A. García-González,²⁸ V. Gavrilov,³² W. Geng,^{12,57} C.E. Gerber,⁴⁶ Y. Gershtein,⁶⁰ G. Ginther,^{45,63} O. Gogota,³⁸ G. Golovanov,³¹ P.D. Grannis,⁶⁴ S. Greder,¹⁶ H. Greenlee,⁴⁵ G. Grenier,¹⁷ Ph. Gris,¹⁰ J.-F. Grivaz,¹³ A. Grohsjean^c,¹⁵ S. Grünendahl,⁴⁵ M.W. Grünewald,²⁶ T. Guillemin,¹³ G. Gutierrez,⁴⁵ P. Gutierrez,⁶⁷ J. Haley,⁶⁸ L. Han,⁴ K. Harder,⁴¹ A. Harel,⁶³ J.M. Hauptman,⁵² J. Hays,⁴⁰ T. Head,⁴¹ T. Hebbeker,¹⁸ D. Hedin,⁴⁷ H. Hegab,⁶⁸ A.P. Heinson,⁴³ U. Heintz,⁶⁹ C. Hensel,¹ I. Heredia-De La Cruz^d,²⁸ K. Herner,⁴⁵ G. Hesketh^f,⁴¹ M.D. Hildreth,⁵¹ R. Hirosky,⁷³ T. Hoang,⁴⁴ J.D. Hobbs,⁶⁴ B. Hoeneisen,⁹ J. Hogan,⁷² M. Hohlfeld,²¹ J.L. Holzbauer,⁵⁸ I. Howley,⁷⁰ Z. Hubacek,^{7,15} V. Hynek,⁷ I. Iashvili,⁶² Y. Ilchenko,⁷¹ R. Illingworth,⁴⁵ A.S. Ito,⁴⁵ S. Jabeen^m,⁴⁵ M. Jaffré,¹³ A. Jayasinghe,⁶⁷ M.S. Jeong,²⁷ R. Jesik,⁴⁰ P. Jiang,⁴ K. Johns,⁴² E. Johnson,⁵⁷ M. Johnson,⁴⁵ A. Jonckheere,⁴⁵ P. Jonsson,⁴⁰ J. Joshi,⁴³ A.W. Jung,⁴⁵ A. Juste,³⁶ E. Kajfasz,¹² D. Karmanov,³³ I. Katsanos,⁵⁹ M. Kaur,²³ R. Kehoe,⁷¹ S. Kermiche,¹² N. Khalatyan,⁴⁵ A. Khanov,⁶⁸ A. Kharchilava,⁶² Y.N. Kharzheev,³¹ I. Kiselevich,³² J.M. Kohli,²³ A.V. Kozelov,³⁴ J. Kraus,⁵⁸ A. Kumar,⁶² A. Kupco,⁸ T. Kurča,¹⁷ V.A. Kuzmin,³³ S. Lammers,⁴⁹ P. Lebrun,¹⁷ H.S. Lee,²⁷ S.W. Lee,⁵² W.M. Lee,⁴⁵ X. Lei,⁴² J. Lellouch,¹⁴ D. Li,¹⁴ H. Li,⁷³ L. Li,⁴³ Q.Z. Li,⁴⁵ J.K. Lim,²⁷ D. Lincoln,⁴⁵ J. Linnemann,⁵⁷ V.V. Lipaev,³⁴ R. Lipton,⁴⁵ H. Liu,⁷¹ Y. Liu,⁴ A. Lobodenko,³⁵ M. Lokajicek,⁸ R. Lopes de Sa,⁴⁵ R. Luna-Garcia^g,²⁸ A.L. Lyon,⁴⁵ A.K.A. Maciel,¹ R. Madar,¹⁹ R. Magaña-Villalba,²⁸ S. Malik,⁵⁹ V.L. Malyshev,³¹ J. Mansour,²⁰ J. Martínez-Ortega,²⁸ R. McCarthy,⁶⁴ C.L. McGivern,⁴¹ M.M. Meijer,^{29,30} A. Melnitchouk,⁴⁵ D. Menezes,⁴⁷ P.G. Mercadante,³ M. Merkin,³³ A. Meyer,¹⁸ J. Meyerⁱ,²⁰ F. Miconi,¹⁶ N.K. Mondal,²⁵ M. Mulhearn,⁷³ E. Nagy,¹² M. Narain,⁶⁹ R. Nayyar,⁴² H.A. Neal,⁵⁶ J.P. Negret,⁵ P. Neustroev,³⁵ H.T. Nguyen,⁷³ T. Nunnemann,²² J. Orduna,⁷² N. Osman,¹² J. Osta,⁵¹ A. Pal,⁷⁰ N. Parashar,⁵⁰ V. Parihar,⁶⁹ S.K. Park,²⁷ R. Partridge^e,⁶⁹ N. Parua,⁴⁹ A. Patwa^j,⁶⁵ B. Penning,⁴⁵ M. Perfilov,³³ Y. Peters,⁴¹ K. Petridis,⁴¹ G. Petrillo,⁶³ P. Pétrouff,¹³ M.-A. Pleier,⁶⁵ V.M. Podstavkov,⁴⁵ A.V. Popov,³⁴ M. Prewitt,⁷² D. Price,⁴¹ N. Prokopenko,³⁴ J. Qian,⁵⁶ A. Quadt,²⁰ B. Quinn,⁵⁸ P.N. Ratoff,³⁹ I. Razumov,³⁴ I. Ripp-Baudot,¹⁶ F. Rizatdinova,⁶⁸ M. Rominsky,⁴⁵ A. Ross,³⁹ C. Royon,¹⁵ P. Rubinov,⁴⁵ R. Ruchti,⁵¹ G. Sajot,¹¹ A. Sánchez-Hernández,²⁸ M.P. Sanders,²² A.S. Santos^h,¹ G. Savage,⁴⁵ M. Savitskyi,³⁸ L. Sawyer,⁵⁴ T. Scanlon,⁴⁰ R.D. Schamberger,⁶⁴ Y. Scheglov,³⁵ H. Schellman,⁴⁸ C. Schwanenberger,⁴¹ R. Schwienhorst,⁵⁷ J. Sekaric,⁵³ H. Severini,⁶⁷ E. Shabalina,²⁰ V. Shary,¹⁵ S. Shaw,⁴¹ A.A. Shchukin,³⁴ V. Simak,⁷ P. Skubic,⁶⁷ P. Slattey,⁶³ D. Smirnov,⁵¹ G.R. Snow,⁵⁹ J. Snow,⁶⁶ S. Snyder,⁶⁵ S. Söldner-Rembold,⁴¹ L. Sonnenschein,¹⁸ K. Soustruznik,⁶ J. Stark,¹¹ D.A. Stoyanova,³⁴ M. Strauss,⁶⁷ L. Suter,⁴¹ P. Svoisky,⁶⁷ M. Titov,¹⁵ V.V. Tokmenin,³¹ Y.-T. Tsai,⁶³ D. Tsybychev,⁶⁴ B. Tuchming,¹⁵ C. Tully,⁶¹ L. Uvarov,³⁵ S. Uvarov,³⁵ S. Uzunyan,⁴⁷ R. Van Kooten,⁴⁹ W.M. van Leeuwen,²⁹ N. Varelas,⁴⁶ E.W. Varnes,⁴² I.A. Vasilyev,³⁴ A.Y. Verkheev,³¹ L.S. Vertogradov,³¹ M. Verzocchi,⁴⁵ M. Vesterinen,⁴¹ D. Vilanova,¹⁵ P. Vokac,⁷ H.D. Wahl,⁴⁴ M.H.L.S. Wang,⁴⁵ J. Warchol,⁵¹ G. Watts,⁷⁴ M. Wayne,⁵¹ J. Weichert,²¹ L. Welty-Rieger,⁴⁸

M.R.J. Williams^{n,49} G.W. Wilson,⁵³ M. Wobisch,⁵⁴ D.R. Wood,⁵⁵ T.R. Wyatt,⁴¹ Y. Xie,⁴⁵ R. Yamada,⁴⁵ S. Yang,⁴ T. Yasuda,⁴⁵ Y.A. Yatsunenkov,³¹ W. Ye,⁶⁴ Z. Ye,⁴⁵ H. Yin,⁴⁵ K. Yip,⁶⁵ S.W. Youn,⁴⁵ J.M. Yu,⁵⁶ J. Zennamo,⁶² T.G. Zhao,⁴¹ B. Zhou,⁵⁶ J. Zhu,⁵⁶ M. Zielinski,⁶³ D. Zieminska,⁴⁹ and L. Zivkovic¹⁴

(The D0 Collaboration*)

¹LAFEX, Centro Brasileiro de Pesquisas Físicas, Rio de Janeiro, Brazil

²Universidade do Estado do Rio de Janeiro, Rio de Janeiro, Brazil

³Universidade Federal do ABC, Santo André, Brazil

⁴University of Science and Technology of China, Hefei, People's Republic of China

⁵Universidad de los Andes, Bogotá, Colombia

⁶Charles University, Faculty of Mathematics and Physics,
Center for Particle Physics, Prague, Czech Republic

⁷Czech Technical University in Prague, Prague, Czech Republic

⁸Institute of Physics, Academy of Sciences of the Czech Republic, Prague, Czech Republic

⁹Universidad San Francisco de Quito, Quito, Ecuador

¹⁰LPC, Université Blaise Pascal, CNRS/IN2P3, Clermont, France

¹¹LPSC, Université Joseph Fourier Grenoble 1, CNRS/IN2P3,
Institut National Polytechnique de Grenoble, Grenoble, France

¹²CPPM, Aix-Marseille Université, CNRS/IN2P3, Marseille, France

¹³LAL, Université Paris-Sud, CNRS/IN2P3, Orsay, France

¹⁴LPNHE, Universités Paris VI and VII, CNRS/IN2P3, Paris, France

¹⁵CEA, Irfu, SPP, Saclay, France

¹⁶IPHC, Université de Strasbourg, CNRS/IN2P3, Strasbourg, France

¹⁷IPNL, Université Lyon 1, CNRS/IN2P3, Villeurbanne, France and Université de Lyon, Lyon, France

¹⁸III. Physikalisches Institut A, RWTH Aachen University, Aachen, Germany

¹⁹Physikalisches Institut, Universität Freiburg, Freiburg, Germany

²⁰II. Physikalisches Institut, Georg-August-Universität Göttingen, Göttingen, Germany

²¹Institut für Physik, Universität Mainz, Mainz, Germany

²²Ludwig-Maximilians-Universität München, München, Germany

²³Panjab University, Chandigarh, India

²⁴Delhi University, Delhi, India

²⁵Tata Institute of Fundamental Research, Mumbai, India

²⁶University College Dublin, Dublin, Ireland

²⁷Korea Detector Laboratory, Korea University, Seoul, Korea

²⁸CINVESTAV, Mexico City, Mexico

²⁹Nikhef, Science Park, Amsterdam, the Netherlands

³⁰Radboud University Nijmegen, Nijmegen, the Netherlands

³¹Joint Institute for Nuclear Research, Dubna, Russia

³²Institute for Theoretical and Experimental Physics, Moscow, Russia

³³Moscow State University, Moscow, Russia

³⁴Institute for High Energy Physics, Protvino, Russia

³⁵Petersburg Nuclear Physics Institute, St. Petersburg, Russia

³⁶Institució Catalana de Recerca i Estudis Avançats (ICREA) and Institut de Física d'Altes Energies (IFAE), Barcelona, Spain

³⁷Uppsala University, Uppsala, Sweden

³⁸Taras Shevchenko National University of Kyiv, Kiev, Ukraine

³⁹Lancaster University, Lancaster LA1 4YB, United Kingdom

⁴⁰Imperial College London, London SW7 2AZ, United Kingdom

⁴¹The University of Manchester, Manchester M13 9PL, United Kingdom

⁴²University of Arizona, Tucson, Arizona 85721, USA

⁴³University of California Riverside, Riverside, California 92521, USA

⁴⁴Florida State University, Tallahassee, Florida 32306, USA

⁴⁵Fermi National Accelerator Laboratory, Batavia, Illinois 60510, USA

⁴⁶University of Illinois at Chicago, Chicago, Illinois 60607, USA

⁴⁷Northern Illinois University, DeKalb, Illinois 60115, USA

⁴⁸Northwestern University, Evanston, Illinois 60208, USA

⁴⁹Indiana University, Bloomington, Indiana 47405, USA

⁵⁰Purdue University Calumet, Hammond, Indiana 46323, USA

⁵¹University of Notre Dame, Notre Dame, Indiana 46556, USA

⁵²Iowa State University, Ames, Iowa 50011, USA

⁵³University of Kansas, Lawrence, Kansas 66045, USA

⁵⁴Louisiana Tech University, Ruston, Louisiana 71272, USA

⁵⁵Northeastern University, Boston, Massachusetts 02115, USA

⁵⁶University of Michigan, Ann Arbor, Michigan 48109, USA

⁵⁷Michigan State University, East Lansing, Michigan 48824, USA

⁵⁸University of Mississippi, University, Mississippi 38677, USA

⁵⁹University of Nebraska, Lincoln, Nebraska 68588, USA

⁶⁰Rutgers University, Piscataway, New Jersey 08855, USA

⁶¹Princeton University, Princeton, New Jersey 08544, USA

⁶²State University of New York, Buffalo, New York 14260, USA

⁶³University of Rochester, Rochester, New York 14627, USA

⁶⁴State University of New York, Stony Brook, New York 11794, USA

⁶⁵Brookhaven National Laboratory, Upton, New York 11973, USA

⁶⁶Langston University, Langston, Oklahoma 73050, USA

⁶⁷University of Oklahoma, Norman, Oklahoma 73019, USA

⁶⁸Oklahoma State University, Stillwater, Oklahoma 74078, USA

⁶⁹Brown University, Providence, Rhode Island 02912, USA

⁷⁰University of Texas, Arlington, Texas 76019, USA

⁷¹Southern Methodist University, Dallas, Texas 75275, USA

⁷²Rice University, Houston, Texas 77005, USA

⁷³University of Virginia, Charlottesville, Virginia 22904, USA

⁷⁴University of Washington, Seattle, Washington 98195, USA

(Dated: February 4, 2015)

We present a measurement of the cross sections for the associated production of a W boson with at least one heavy quark jet, b or c , in proton-antiproton collisions. Data corresponding to an integrated luminosity of 8.7 fb^{-1} recorded with the D0 detector at the Fermilab Tevatron $p\bar{p}$ Collider at $\sqrt{s} = 1.96 \text{ TeV}$ are used to measure the cross sections differentially as a function of the jet transverse momenta in the range 20 to 150 GeV. These results are compared to calculations of perturbative QCD theory as well as predictions from Monte Carlo generators.

PACS numbers: 12.38.Qk, 13.85.Qk, 14.65.Fy, 14.70.Fm

Measurement of the production cross section of a W boson in association with a b or c -quark jet provides a stringent test of quantum chromodynamics (QCD). At hadron colliders, the associated production of a heavy quark with a W boson can also be a significant background to rare standard model (SM) processes, for example, production of top quark pairs [1], a single top quark [2], and a W boson in association with a Higgs boson decaying to two b quarks [3], as well as for new physics processes, e.g., supersymmetric scalar top quark production [4].

The dominant processes contributing to $W + c$ -jet production are $qg \rightarrow Wc$ and $q\bar{q}' \rightarrow Wg$ followed by $g \rightarrow c\bar{c}$. The production cross section for the first process is sensitive to the quark and gluon parton density functions (PDFs). Since the c - b quark

Cabibbo-Kobayashi-Maskawa matrix element is very small ($|V_{cb}|^2 \approx 0.0016$) [5], the contribution of a b -quark initial state in the PDF is negligible. Comparing the d -quark and s -quark PDFs, the probability of interaction of a gluon with an d -quark is greater than that with a s -quark, but the CKM matrix element suppresses $d \rightarrow c$ transitions since $|V_{cd}|^2 \approx 0.04$. As a result, the expected contributions from s -quark and d -quark initial states for a jet transverse momentum $p_T^{\text{jet}} > 20 \text{ GeV}$ at the Tevatron are around 85% and 15%, respectively [6]. According to the ALPGEN+PYTHIA [7, 8] simulation for $W + c$ -jet events, the contribution from $qg \rightarrow W + c$ dominates the entire $20 < p_T^{\text{jet}} < 100 \text{ GeV}$ region with the contribution from $q\bar{q}' \rightarrow W + c\bar{c}$ events increasing from about 25% to 45% as jet p_T increases from 20 to 100 GeV. Measurement of the $p\bar{p} \rightarrow W + c$ -jet differential cross section should provide information about the s -quark PDF. This PDF has been measured directly only in fixed target neutrino-nucleon deep inelastic scattering experiments at relatively low momentum transfer $Q \lesssim 15 - 20 \text{ GeV}$ [9–14]. A probe of the s -quark PDF at the Tevatron tests the universality of $s(x, Q^2)$, where x is the Feynman variable [15], and its QCD evolution up to $Q^2 \simeq 10^4 \text{ GeV}^2$.

There are only a few previous measurements of the $W + c$ -jet cross section at hadron colliders, performed by the D0 [6], CDF [16, 17], ATLAS [18], and CMS [19] Collaborations. The previous D0 and CDF measurements are inclusive; the CMS and ATLAS inclusive results were augmented by distributions in the pseudorapidity of the lepton from W decay. It is important to note that the

*with visitors from ^aAugustana College, Sioux Falls, SD, USA, ^bThe University of Liverpool, Liverpool, UK, ^cDESY, Hamburg, Germany, ^dUniversidad Michoacana de San Nicolas de Hidalgo, Morelia, Mexico ^eSLAC, Menlo Park, CA, USA, ^fUniversity College London, London, UK, ^gCentro de Investigacion en Computacion - IPN, Mexico City, Mexico, ^hUniversidade Estadual Paulista, São Paulo, Brazil, ⁱKarlsruher Institut für Technologie (KIT) - Steinbuch Centre for Computing (SCC), D-76128 Karlsruhe, Germany, ^jOffice of Science, U.S. Department of Energy, Washington, D.C. 20585, USA, ^kAmerican Association for the Advancement of Science, Washington, D.C. 20005, USA, ^lKiev Institute for Nuclear Research, Kiev, Ukraine, ^mUniversity of Maryland, College Park, Maryland 20742, USA and ⁿEuropean Organization for Nuclear Research (CERN), Geneva, Switzerland

measurements listed above are performed by requiring opposite electric charges of a soft lepton inside a jet from semileptonic charmed hadron decay with a lepton from W decay elsewhere in the event, and measuring the cross section for “opposite-sign” (OS) minus “same-sign” (SS) events. A requirement of opposite signs for the leptons and subtraction of events with the same signs suppresses the sign-symmetric backgrounds as well as $W + c\bar{c}$ events due to gluon splitting, which become significant at high jet p_T . All measurements are in agreement with the perturbative next-to-leading order (NLO) QCD predictions [20, 21] that include contributions from gluon splitting within total theoretical uncertainties of 15–30%.

Measurements of the inclusive $W + b$ -jet cross-sections have been reported by the CDF [22], D0 [23], and ATLAS [24] Collaborations. The CDF result is approximately 3σ higher than the NLO predictions while the D0 and ATLAS measurements agree with the theory within large (30–40%) theoretical uncertainties. A dominant ($\simeq 85\%$) contribution to $W + b$ -jet production at the Tevatron is due to the $q\bar{q}' \rightarrow W + g$ ($g \rightarrow b\bar{b}$) process while the remaining contribution arises from the $b\bar{q} \rightarrow Wb\bar{q}'$ process [21], with a negligible contribution from single top quark production.

We present, for the first time, measurements of $W + c$ -jet and $W + b$ -jet differential cross sections as a function of jet p_T , where no requirement of a soft lepton within a jet is made, and that are therefore sensitive to the gluon splitting contributions. The W boson candidates are identified in the $\mu + \nu$ decay channel.

The data used in this analysis were collected between July 2006 and September 2011 using the D0 detector at the Fermilab Tevatron Collider at $\sqrt{s} = 1.96$ TeV, and correspond to an integrated luminosity of 8.7 fb^{-1} . The D0 detector [25] has a central tracking system consisting of a silicon microstrip tracker (SMT) [26] and a central fiber tracker, both located within a 1.9 T superconducting solenoidal magnet, which are optimized for tracking and vertexing at pseudorapidities $|\eta| < 3$ and $|\eta| < 2.5$, respectively [27]. A liquid argon and uranium calorimeter has a central section (CC) covering pseudorapidities $|\eta| \lesssim 1.1$, and two end calorimeters (EC) that extend coverage to $|\eta| \approx 4.2$, with all three housed in separate cryostats [28]. An outer muon system covering $|\eta| < 2$ consists of a layer of tracking detectors and scintillation trigger counters in front of 1.8 T iron toroids, followed by two similar layers after the toroids. Luminosity is measured using plastic scintillator arrays located in front of the EC cryostats.

The $W + b/c$ candidate events are chosen by selecting single muon or muon+jet signatures with a three-level trigger system. The trigger efficiency has been estimated using $Z \rightarrow \mu^+\mu^-$ (+jets) events in data. The trigger efficiency is parametrized as a function of muon p_T and η and is on average $\approx 70\%$.

Offline event selection requires a reconstructed $p\bar{p}$ in-

teraction primary vertex (PV) that has at least three associated tracks and is located within 60 cm of the center of the detector along the beam direction. The vertex selection for $W + b/c$ events is approximately 99% efficient as measured in simulation.

We require a muon candidate to be reconstructed from hits in the muon system and matched to a reconstructed track in the central tracker [29]. The transverse momentum of the muon must satisfy $p_T^\mu > 20$ GeV, with $|\eta^\mu| < 1.7$. Muons are required to be spatially isolated from other energetic particles using information from the central tracking detectors and calorimeter [30]. Muons from cosmic rays are rejected by applying a timing criterion on the hits in the scintillator layers of the muon system and by applying restrictions on the displacement of the muon track with respect to the PV. The muon reconstruction efficiency is $\approx 90\%$.

Candidate $W + jets$ events are selected by requiring at least one reconstructed jet with pseudorapidity $|\eta^{\text{jet}}| < 1.5$ and $p_T^{\text{jet}} > 20$ GeV. Jets are reconstructed from energy deposits in the calorimeter using the iterative midpoint cone algorithm [31] with a cone of radius $R = \sqrt{\Delta\eta^2 + \Delta\phi^2} = 0.5$ [27]. The energies of jets are corrected for detector response, the presence of noise and multiple $p\bar{p}$ interactions [32]. To enrich the sample with W bosons, events are required to have missing transverse energy [32] $\cancel{E}_T > 25$ GeV due to the neutrino escaping detection. We require that the W boson candidates have a transverse mass $M_T > 40$ GeV [33].

Backgrounds for this analysis include events from the production of $W + \text{light parton jets}$, $Z/\gamma^* + \text{jets}$, $t\bar{t}$, single top quark, diboson VV ($V = W, Z$) and QCD multijets in which a jet is misidentified as a muon. The $W + c$ and $W + b$ signal and the background processes excluding multijet are simulated using a combination of ALPGEN [7] and PYTHIA [8] MC event generators with PYTHIA providing parton showering and hadronization. We use PYTHIA with CTEQ6L1 [34] PDFs. ALPGEN generates multi-parton final states using tree-level matrix elements (ME). When interfaced with PYTHIA, it employs the MLM scheme [7] to treat ME partons produced from showering in PYTHIA. For the signal process, we also use the SHERPA MC generator [35] that matches partons from the leading-order ME with up to two real parton emissions to the parton-shower jets according to the CKWK matching scheme [36]. The generated events are processed through a GEANT-based [37] simulation of the D0 detector geometry and response. To accurately model the effects of multiple $p\bar{p}$ interactions and detector noise, events from random $p\bar{p}$ crossings with a similar instantaneous luminosity spectrum as in data are overlaid on the MC events. These MC events are then processed using the same reconstruction code as for the data. The MC events are also weighted to take into account the trigger efficiency and small observed differences between MC and data in the distributions of the instantaneous luminosity

and of the z coordinate of the $p\bar{p}$ collision vertex.

The V +jets processes are normalized to the total inclusive W and Z -boson cross sections calculated at NNLO (next-to-next-to-leading order) [38]. The Z -boson p_T distribution is modeled to match the distribution observed in data [39], taking into account the dependence on the number of reconstructed jets. To reproduce the W -boson p_T distribution in simulated events, we use the product of the measured Z -boson p_T spectrum times the ratio of W to Z -boson p_T distributions at NLO [39, 40]. The NLO+NNLL (next-to-next-to-leading log) calculations are used to normalize $t\bar{t}$ production [41], while single top quark production is normalized to NNLO predictions [42]. The NLO WW , WZ , and ZZ production cross section values are obtained with the MCFM program [43]. The multijet background contribution is estimated from data using the “matrix method” [30]. For the final states studied here the multijet background is small ($\lesssim 2\%$) and arises mainly from the semileptonic decays of heavy quarks in which the muon satisfies the isolation requirements. To reduce the contribution from $t\bar{t}$ production that increases with jet p_T , we restrict the scalar sum of all the jet p_T values (H_T) to be less than 175 GeV. This requirement reduces the $t\bar{t}$ fraction by a factor 1.5 – 2, depending on jet p_T , and has signal efficiency greater than 95% except in the highest H_T bin where it falls to 82%. The $t\bar{t}$ fraction after the H_T cut varies between 5 and 20% with increasing jet p_T .

Identification of b and c jets is crucial for this measurement. Once the inclusive W + jets sample is selected, at least one jet is required to be taggable, i.e. it must contain at least two tracks each with at least one hit in the SMT, $p_T > 1$ GeV for the highest- p_T track and $p_T > 0.5$ GeV for the next-to-highest p_T track. These criteria ensure sufficient information to classify the jet as a heavy-flavor candidate and have a typical efficiency of about 90%. Light parton jets (those resulting from light quarks or gluons) are suppressed using a dedicated artificial neural network (b -NN) [44] that exploits the longer lifetimes of heavy-flavor hadrons relative to their lighter counterparts. The inputs to the b -NN include several characteristic quantities of the jet and associated tracks to provide a continuous output value that tends towards one for b jets and zero for the light jets. The b -NN input variables providing most of the discrimination are the number of reconstructed secondary vertices (SV) in the jet, the invariant mass of charged particle tracks associated with the SV (M_{SV}), the number of tracks used to reconstruct the SV, the two-dimensional decay length significance of the SV in the plane transverse to the beam, a weighted combination of the tracks’ transverse impact parameter significances, and the probability that the tracks associated with the jet originate from the $p\bar{p}$ interaction vertex, which is referred to as the jet lifetime probability (JLIP). The jet is required to have a b -NN output greater than 0.5. For jet p_T in a range between

20 and 150 GeV this selection is (36 – 47)% efficient for b -jets and (8 – 11)% efficient for c jets with relative systematic uncertainties of (4.2 – 6.5)% for both the b jets and c jets. The systematic uncertainty is obtained from a comparison of the heavy flavor tagging efficiencies in data and MC as described in [44]. Only 0.2 – 0.4% of light jets are misidentified as heavy-flavor jets and comprise 7% to 15% of the final sample, with a larger fraction at lower jet p_T . In addition to the b -NN output, we obtain further information by combining the M_{SV} and JLIP variables, which provide good discrimination between b , c , and light quark jets due to their different masses [45, 46]. We form a single variable discriminant $\mathcal{D}_{\text{MJL}} = \frac{1}{2} (M_{SV}/(5 \text{ GeV}) - \ln(\text{JLIP})/20)$ [45] and require $\mathcal{D}_{\text{MJL}} > 0.1$ to remove poorly reconstructed events and reduce the number of light-jet events. The efficiency for signal events to pass this selection is 98% for b -jets and 97% for c -jets.

After all selection requirements, 5260 events remain in the data sample. We measure the fraction of $W + c$ and $W + b$ events in the selected sample by performing a binned maximum likelihood fit to the observed data distribution of the \mathcal{D}_{MJL} discriminant in bins of jet p_T , as shown in Fig. 1 for the bin $30 < p_T^{\text{jet}} < 40$ GeV. The templates for $W + b$ and $W + c$ jets are taken from the simulation. Expected contributions from the background processes are subtracted from the \mathcal{D}_{MJL} distribution in data before the fit. The ratio of the W +light parton jets to W + all jet flavors has been estimated using ALPGEN+PYTHIA MC events taking into account the data-to-MC correction factors as described in Ref. [44], and has been cross checked in data using looser cuts on b -NN output in the range from 0.15–0.3.

The fractions of $W + b$ and $W + c$ events after subtraction of background contribution are shown in Fig. 2 as a function of jet p_T . The relative uncertainties on the fractions obtained from the fit range within (7 – 13)% for $W + b$ and (6 – 11)% for $W + c$. This includes the uncertainty due to $W + b$ and $W + c$ template shapes, studied in a previous analysis [47]. The contributions from the background events are varied within uncertainties on their predicted cross sections, and these uncertainties are propagated into the extracted signal fractions. The uncertainty due to the light parton jets template shape is taken from Ref. [46]. The overall relative uncertainties on the subtracted backgrounds range within (4 – 6)% for $W + b$ and (3 – 4)% for $W + c$.

We apply corrections to the measured number of signal events to account for the detector and kinematic acceptances and selection efficiencies using simulated samples of $W + b(c)$ -jet events. In these calculations, we apply the following selections at the particle level: at least one $b(c)$ -jet with $p_T^{b(c)\text{-jet}} > 20$ GeV, $|\eta^{b(c)\text{-jet}}| < 1.5$, a muon with $p_T^\mu > 20$ GeV and $|\eta^\mu| < 1.7$, and a neutrino with $p_T^\nu > 25$ GeV. In the following, we quote our cross section results for this restricted phase space as a fiducial cross

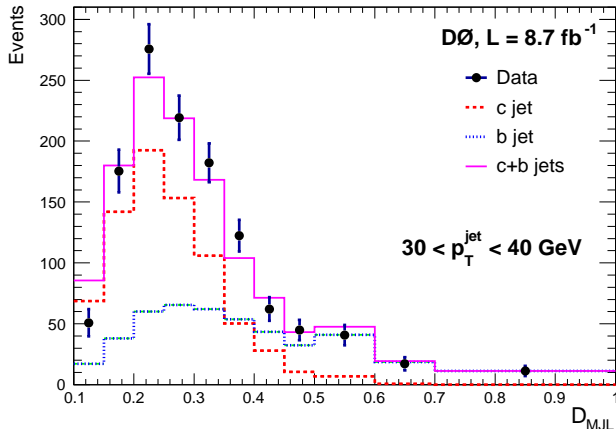


FIG. 1: (Color online) Distribution of the D_{MJL} discriminant after all selection criteria (including b -NN output > 0.5) for a representative bin of $30 < p_T^{\text{jet}} < 40$ GeV. The contributions from background events are subtracted from data before the fit. The distributions for the c -jet and b -jet templates (with statistical uncertainties) are shown normalized to their respective fitted fractions.

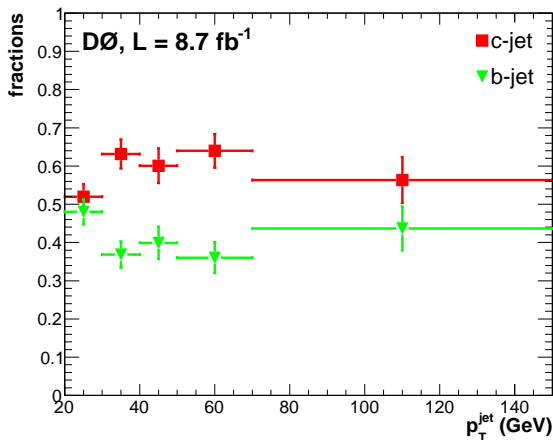


FIG. 2: (Color online) The b - and c -jet fractions (their total sum is normalized to 1.0) versus jet p_T with total uncertainty from the D_{MJL} fit.

section.

The acceptance is defined by the selection requirements in jet and muon transverse momenta and pseudorapidities. Correction factors to account for small differences between jet- p_T and rapidity spectra in data and simulation are estimated, and used as weights to create a data-like MC sample. The differences between acceptance corrections obtained with standard and corrected MC samples are taken as a systematic uncertainty of up to 3% at low jet p_T . An additional systematic uncertainty of up to 4% is due to uncertainties in the jet energy correction and resolution. For $20 < p_T^{\text{jet}} < 150$ GeV

the product of acceptance and muon selection efficiency varies within (50 – 65)% with a relative systematic uncertainty of (3 – 5)%. The systematic uncertainty on the muon selection efficiency is about 2% and is obtained from a comparison of the muon efficiencies in $Z \rightarrow \mu\mu$ events in data and MC. Uncertainties on b -jet identification are determined in simulations and data by using b -jet-enriched samples [44] and are about (2 – 5)% per jet. The integrated luminosity is known to a precision of 6.1% [48]. By summing the uncertainties in quadrature we obtain a final total systematic uncertainty on the cross section measurements of (11 – 18)% depending on jet p_T and final state.

To check the stability of the results, the $W + b$ -jet and $W + c$ -jet cross sections have been remeasured using a looser b -NN selection, b -NN output > 0.3 , and with the light parton jet fraction included as an additional fit parameter, thus increasing the data statistics and the background fractions. The fractions of b - and c -jets are obtained from the maximum likelihood fit of the light, b - and c -jet templates to D_{MJL} distribution in data as shown in Fig. 3. We also vary the default H_T cut by ± 15 GeV and remeasure the cross sections. In both cross-checks, the default and new cross sections are found to be in agreement within uncertainties that include the correlation between the two measurements.

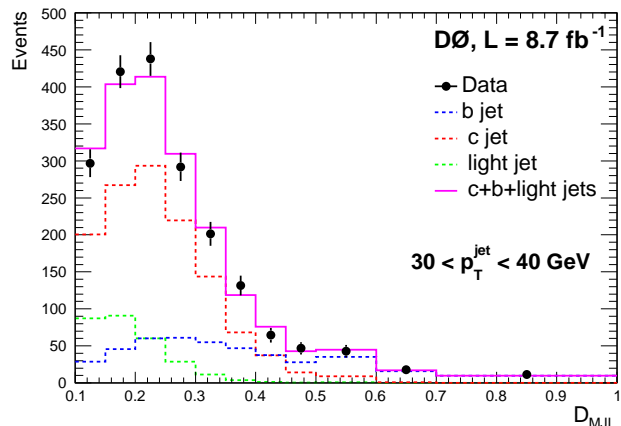


FIG. 3: (Color online) Similar to Fig. 1 but for events selected with b -NN output > 0.3 . This alternative selection is used as a cross-check of the main results.

In Figs. 4 and 5 and Tables I and II, we present the $W + b$ -jet and $W + c$ -jet differential production cross sections times $W \rightarrow \mu\nu$ branching fraction for the fiducial phase space defined by $p_T^\mu > 20$ GeV, $|\eta^\mu| < 1.7$, $p_T^\nu > 25$ GeV, and with at least one $b(c)$ -jet with $p_T^{\text{jet}} > 20$ GeV and $|\eta^{\text{jet}}| < 1.5$. The cross sections are presented differentially in five p_T^{jet} bins in the region 20 – 150 GeV. The data points are plotted at the value of p_T^{jet} for which the value of a smooth function describing the cross section equals the averaged cross section in the bin [49].

The cross sections are compared to predictions from NLO QCD [43] and two MC generators, SHERPA and ALPGEN. The NLO predictions are made using the MSTW2008 [50] and CT10 [51] PDF sets. We calculate the NLO QCD prediction using MCFM with central values of renormalization and fragmentation scales $\mu_r = \mu_f = M_W$ and with the b -quark and c -quark masses $m_b = 4.75$ GeV and $m_c = 1.5$ GeV, respectively. Uncertainties are estimated by varying μ_r and μ_f independently by a factor of two in each direction.

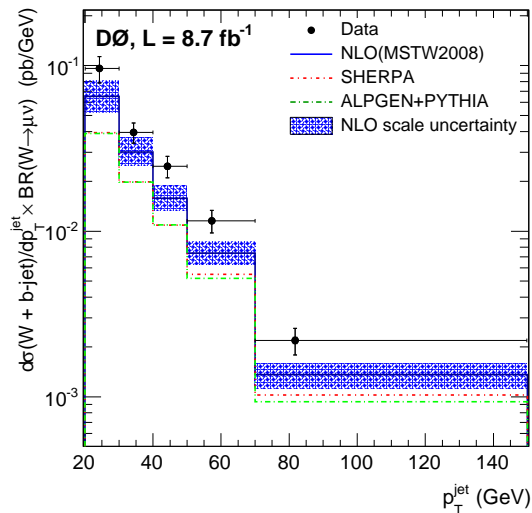


FIG. 4: (Color online) The $W + b$ -jet differential production cross section times $W \rightarrow \mu\nu$ branching fraction as a function of jet p_T . The uncertainties on the data points include statistical and systematic contributions added in quadrature. The measurements are compared to the NLO QCD calculations [43] using the MSTW2008 PDF set [50] (solid line). The predictions from SHERPA [35] and ALPGEN [7] are shown by the dotted and dashed lines, respectively.

The NLO predictions are corrected for non-perturbative effects such as parton-to-hadron fragmentation and multiple parton interactions. The latter are evaluated using SHERPA and PYTHIA MC samples generated using their default settings [8, 35]. The overall corrections vary within a factor of 0.80 – 1.1 with an uncertainty of $\lesssim 5\%$ assigned to account for the difference between the two MC generators. The ratios of data over the NLO QCD calculations and of the various theoretical predictions to the NLO QCD calculations are presented in Figs. 6 and 7. The measured $W + b$ -jet cross sections are systematically above the NLO QCD predictions for all jet p_T bins. The $W + c$ -jet data agree with the NLO QCD predictions at small p_T but disagree at higher p_T as the contribution from $q\bar{q}' \rightarrow W + g$ ($g \rightarrow c\bar{c}$) events increases.

In addition to measuring the $W + b$ -jet and $W + c$ -jet cross-sections, we calculate the ratio $\sigma(W + c)/\sigma(W + b)$

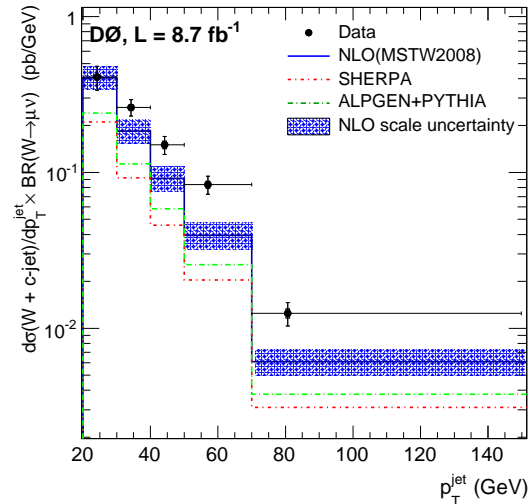


FIG. 5: (Color online) The $W + c$ -jet differential production cross section times $W \rightarrow \mu\nu$ branching fraction as a function of jet p_T . The uncertainties on the data points include statistical and systematic contributions added in quadrature. The measurements are compared to the NLO QCD calculations [43] using the MSTW2008 PDF set [50] (solid line). The predictions from SHERPA [35] and ALPGEN [8] are shown by the dotted and dashed lines, respectively.

in jet p_T bins. In this ratio, many experimental systematic uncertainties cancel. Also, theory predictions of the ratio are less sensitive to the scale uncertainties and effects from missing higher-order terms that impact the normalizations of the cross sections. The remaining uncertainties are caused by largely anti-correlated uncertainties coming from the fitting of c -jet and b -jet D_{MJL} templates to data, and by other uncertainties on the b - and c -jet fractions discussed above. Experimental results as well as theoretical predictions for the ratios are presented in Table III and Fig. 8. The systematic uncertainties on the ratio vary within (11 – 17)%. Theoretical scale uncertainties, estimated by varying the renormalization and factorization scales by a factor of two in the same way for the $\sigma(W + b)$ and $\sigma(W + c)$ predictions, are also significantly reduced. Specifically, residual scale uncertainties are typically (0.5 – 4.6)% for NLO QCD, which indicates a much smaller dependence of the ratio on the higher-order corrections. The ratio $\sigma(W + c)/\sigma(W + b)$ for $p_T^{\text{jet}} > 30$ GeV is reasonably consistent with theoretical predictions except for SHERPA.

In summary, we have performed the first measurement of the differential cross section as a function of p_T^{jet} for the $W + b$ -jet and $W + c$ -jet final states with $W \rightarrow \mu\nu$ decay at $\sqrt{s} = 1.96$ TeV, in a restricted phase space of $p_T^\mu > 20$ GeV, $|\eta^\mu| < 1.7$, $p_T^\nu > 25$ GeV and with $b(c)$ jets with the p_T range $20 < p_T^{\text{jet}} < 150$ GeV and $|\eta^{\text{jet}}| < 1.5$.

TABLE I: The $W + b$ -jet production cross sections times $W \rightarrow \mu\nu$ branching fraction, $d\sigma/dp_T^{\text{jet}}$, together with statistical uncertainties (δ_{stat}) and total systematic uncertainties (δ_{syst}). The column δ_{tot} shows total experimental uncertainty obtained by adding δ_{stat} and δ_{syst} in quadrature. The last three columns show theoretical predictions obtained using NLO QCD with MSTW PDF set, and two MC event generators, SHERPA and ALPGEN.

p_T^{jet} bin (GeV)	$\langle p_T^{\text{jet}} \rangle$ (GeV)	$d\sigma/dp_T^{\text{jet}}$ (pb/GeV)						
		Data	δ_{stat} (%)	δ_{syst} (%)	δ_{tot} (%)	NLO QCD	SHERPA	ALPGEN
20–30	24.3	9.6×10^{-2}	2.4	17.8	18.0	6.5×10^{-2}	3.9×10^{-2}	3.9×10^{-2}
30–40	34.3	4.0×10^{-2}	2.9	13.6	13.9	3.0×10^{-2}	2.0×10^{-2}	2.0×10^{-2}
40–50	44.3	2.5×10^{-2}	3.6	14.4	14.8	1.6×10^{-2}	1.1×10^{-2}	1.1×10^{-2}
50–70	57.2	1.2×10^{-2}	3.4	15.2	15.6	7.4×10^{-3}	5.5×10^{-3}	5.2×10^{-3}
70–150	81.7	2.2×10^{-3}	4.5	17.7	18.3	1.4×10^{-3}	1.0×10^{-3}	9.3×10^{-4}

TABLE II: The $W + c$ -jet production cross sections times $W \rightarrow \mu\nu$ branching fraction, $d\sigma/dp_T^{\text{jet}}$, together with statistical uncertainties (δ_{stat}) and total systematic uncertainties (δ_{syst}). The column δ_{tot} shows total experimental uncertainty obtained by adding δ_{stat} and δ_{syst} in quadrature. The last three columns show theoretical predictions obtained using NLO QCD with MSTW PDF set, and two MC event generators, SHERPA and ALPGEN.

p_T^{jet} bin (GeV)	$\langle p_T^{\text{jet}} \rangle$ (GeV)	$d\sigma/dp_T^{\text{jet}}$ (pb/GeV)						
		Data	δ_{stat} (%)	δ_{syst} (%)	δ_{tot} (%)	NLO QCD	SHERPA	ALPGEN
20–30	24.2	4.1×10^{-1}	3.7	17.0	17.4	4.1×10^{-1}	2.1×10^{-1}	2.4×10^{-1}
30–40	34.2	2.6×10^{-1}	4.6	11.0	11.9	1.8×10^{-1}	9.2×10^{-2}	1.1×10^{-1}
40–50	44.2	1.5×10^{-1}	5.8	11.9	13.2	9.2×10^{-2}	4.6×10^{-2}	5.9×10^{-2}
50–70	57.0	8.4×10^{-2}	5.3	12.1	13.2	3.9×10^{-2}	2.0×10^{-2}	2.6×10^{-2}
70–150	80.7	1.3×10^{-2}	6.9	15.6	17.1	6.1×10^{-3}	3.1×10^{-3}	3.8×10^{-3}

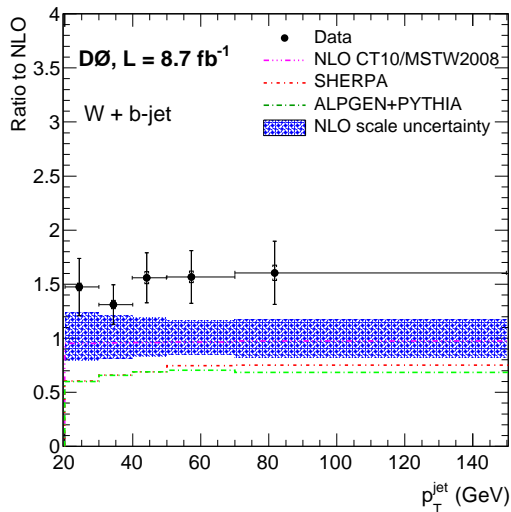


FIG. 6: (Color online) The ratio of $W + b$ -jet production cross sections to NLO predictions with the MSTW2008 PDF set [50] for data and theoretical predictions. The uncertainties on the data include both statistical (inner error bar) and total uncertainties (full error bar). Also shown are the uncertainties on the theoretical QCD scales. The ratio of NLO QCD predictions with CT10 [51] to those obtained with MSTW2008 as well as the predictions given by SHERPA [35] and ALPGEN [7] are also presented.

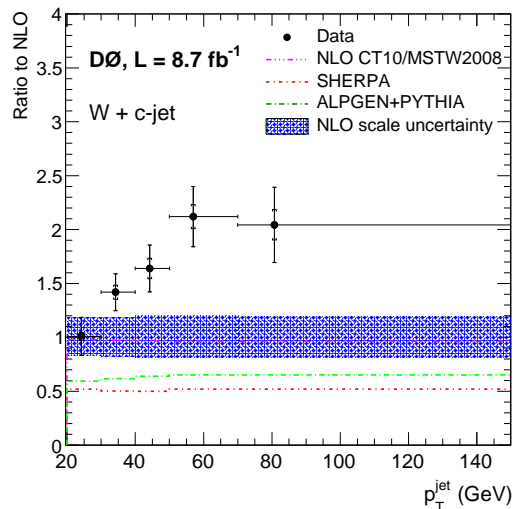


FIG. 7: (Color online) The ratio of $W + c$ -jet production cross sections to NLO predictions with the MSTW2008 PDF set [50] for data and theoretical predictions. The uncertainties on the data include both statistical (inner error bar) and total uncertainties (full error bar). Also shown are the uncertainties on the theoretical QCD scales. The ratio of NLO QCD predictions with CT10 [51] to those obtained with MSTW2008 as well as the predictions given by SHERPA [35] and ALPGEN [7] are also presented.

TABLE III: The $\sigma(W + c)/\sigma(W + b)$ cross section ratio in bins of $c(b)$ -jet p_T together with statistical uncertainties (δ_{stat}), total systematic uncertainties (δ_{syst}). The column δ_{tot} shows total experimental uncertainty obtained by adding δ_{stat} and δ_{syst} in quadrature. The last three columns show theoretical predictions obtained with the NLO QCD using MSTW2008 PDF set, and two MC event generators, SHERPA and ALPGEN.

p_T^{jet} bin (GeV)	$\langle p_T^{\text{jet}} \rangle$ (GeV)	Ratio $\sigma(W + c)/\sigma(W + b)$					NLO QCD	SHERPA	ALPGEN
		Data	δ_{stat} (%)	δ_{syst} (%)	δ_{tot} (%)				
20–30	24.3	4.3	2.9	13.3	13.6	6.2	5.4	6.2	
30–40	34.3	6.6	3.6	12.7	13.2	6.1	4.7	5.7	
40–50	44.3	6.1	4.6	13.9	14.7	5.8	4.2	5.4	
50–70	57.1	7.2	4.2	13.8	14.4	5.3	3.7	4.9	
70–150	81.2	5.7	5.4	17.5	18.3	4.5	3.0	4.1	

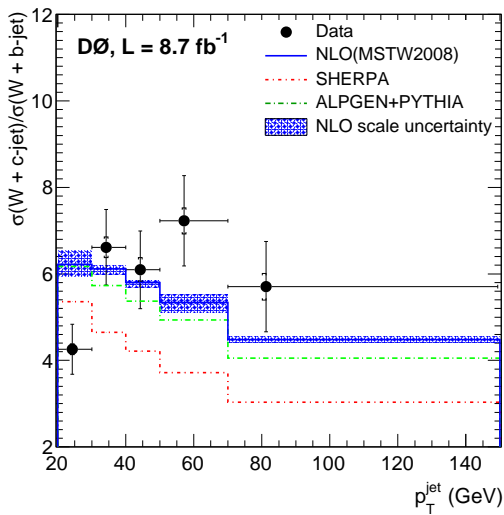


FIG. 8: The ratio of the $W + c$ -jet to $W + b$ -jet production cross sections for data and theory as a function of jet p_T . The uncertainties on the points include both statistical (inner line) and the full uncertainties (the entire error bar). Predictions given by NLO QCD with the MSTW2008 PDF set [50], SHERPA [35] and ALPGEN [7] are also shown.

These are the first measurements of $W + b/c$ cross sections that are sensitive to the gluon splitting processes. The measured $W + b$ -jet cross section is higher than the predictions in all p_T bins and is suggestive of missing higher order corrections. The measured $W + c$ -jet cross section agrees with NLO prediction for the low p_T^{jet} (20–30 GeV), but disagrees towards high p_T^{jet} . The disagreement may be due to missing higher order corrections and an underestimated contribution from gluon splitting $g \rightarrow c\bar{c}$ also observed earlier at LEP [52], LHCb [53], ATLAS [54] and D0 experiments [47, 55], and/or possible enhancement in the strange quark PDF as suggested by CHORUS [56], CMS [19] and ATLAS [18] data according to a recent PDF fit performed by ABKM group [57].

We thank John Campbell for useful discussions and predictions with MCFM. We thank the staffs at Fer-

milab and collaborating institutions, and acknowledge support from the DOE and NSF (USA); CEA and CNRS/IN2P3 (France); MON, NRC KI, and RFBR (Russia); CNPq and FAPERJ (Brazil); DAE and DST (India); COLCIENCIAS (Colombia); CONACYT (Mexico); NRF (Korea); FOM (The Netherlands); STFC and The Royal Society (UK); MSMT (Czech Republic); BMBF and DFG (Germany); SFI (Ireland); Swedish Research Council (Sweden); CAS and CNSF (China); and MESU (Ukraine).

-
- [1] V. M. Abazov *et al.* (D0 Collaboration), Phys. Rev. D **90**, 092006 (2014).
 - [2] V. M. Abazov *et al.* (D0 Collaboration), Phys. Lett. B **726**, 656 (2013).
 - [3] V. M. Abazov *et al.* (D0 Collaboration), Phys. Rev. D **88**, 052008 (2013).
 - [4] V. M. Abazov *et al.* (D0 Collaboration), Phys. Lett. B **710**, 578 (2012); Phys. Lett. B **696**, 321 (2011).
 - [5] K. A. Olive *et al.* (Particle Data Group), Chin. Phys. C **38**, 090001 (2014), *The CKM quark-mixing matrix* review.
 - [6] V. M. Abazov *et al.* (D0 Collaboration), Phys. Lett. B **666**, 23 (2008).
 - [7] M. Mangano *et al.*, J. High Energy Phys. **07** (2003) 001. We use ALPGEN v2.3.
 - [8] T. Sjöstrand *et al.*, Comput. Phys. Commun. 135 (2001) 238. We use pythia v6.409.
 - [9] D.A. Mason *et al.* (NuTeV Collaboration), Phys. Rev. Lett. **99**, 192001 (2007).
 - [10] M. Goncharov *et al.* (NuTeV Collaboration), Phys. Rev. D **64**, 112006 (2001).
 - [11] S. A. Rabinowitz *et al.* (CCFR Collaboration), Phys. Rev. Lett. **70**, 134 (1993).
 - [12] A. O. Bazarko *et al.* (CCFR Collaboration), Z. Phys. C **65**, 189 (1995).
 - [13] P. Vilain *et al.* (Charm II Collaboration), Eur. Phys. J. C **11**, 19 (1999).
 - [14] H. Abramowicz *et al.* (CDHS Collaboration), Z. Phys. C **15**, 19 (1982).
 - [15] R. P. Feynman, Phys. Rev. Lett. **23**, 1415 (1969).
 - [16] T. Aaltonen *et al.* (CDF Collaboration), Phys. Rev. Lett. **100**, 091803 (2008).

- [17] T. Aaltonen *et al.* (CDF Collaboration), Phys. Rev. Lett. **110**, 071801 (2013).
- [18] G. Aad *et al.* (ATLAS Collaboration), J. High Energy Phys. **05** 068 (2014).
- [19] S. Chatrchyan, *et al.* (CMS Collaboration), J. High Energy Phys. **02**, 013 (2014).
- [20] J. Campbell, R. K. Ellis, F. Maltoni, and S. Willenbrock, Phys. Rev. D **75**, 054015 (2007).
- [21] J. Campbell *et al.*, Phys. Rev. D **79**, 034023 (2009).
- [22] T. Aaltonen *et al.* (CDF Collaboration), Phys. Rev. Lett. **104**, 131801 (2010).
- [23] V. M. Abazov *et al.* (D0 Collaboration), Phys. Lett. B **718**, 1314 (2013).
- [24] G. Aad *et al.* (ATLAS Collaboration), Phys. Lett. B **707**, 418 (2012).
- [25] V. M. Abazov *et al.* (D0 Collaboration), Nucl. Instrum. Methods in Phys. Res. A **565**, 463 (2006).
- [26] R. Angstadt *et al.*, Nucl. Instrum. Methods in Phys. Res. Sect. A **622**, 298 (2010).
- [27] We use a standard right-handed coordinate system. The nominal collision point is the center of the detector with coordinates (0, 0, 0). The direction of the proton beam is the $+z$ axis. The $+x$ axis is horizontal, pointing away from the center of the Tevatron ring. The $+y$ axis points vertically upwards. The polar angle, θ , is defined such that $\theta = 0$ is the $+z$ direction. The rapidity is defined as $y = -\ln[(E + p_z)/(E - p_z)]$, where E is the energy and p_z is the momentum component along the proton beam direction. Pseudorapidity is defined as $\eta = -\ln(\tan \frac{\theta}{2})$. ϕ is defined as the azimuthal angle in the plane transverse to the proton beam direction.
- [28] S. Abachi *et al.* (D0 Collaboration), Nucl. Instrum. Methods in Phys. Res. A **324**, 53 (1993).
- [29] V. M. Abazov *et al.* (D0 Collaboration), Nucl. Instrum. Methods in Phys. Res. Sect. A **737**, 281 (2014).
- [30] V. M. Abazov *et al.* (D0 Collaboration), Phys. Rev. D. **86**, 032005 (2012).
- [31] G. C. Blazey *et al.*, arXiv:hep-ex/0005012 (2000). We use the algorithm *ILCA* described in section 3.4.
- [32] V. M. Abazov *et al.* (D0 Collaboration), Nucl. Instrum. Methods in Phys. Res. A **763**, 442 (2014).
- [33] The measured properties of W boson candidates are limited by their transverse energy and transverse mass, defined as $M_T = \sqrt{(\cancel{p}_T + p_T^l)^2 - (\cancel{p}_x + p_x^l)^2 - (\cancel{p}_y + p_y^l)^2}$, where \cancel{p}_T is the magnitude of the missing transverse energy vector, p_T^l is the transverse momentum of the lepton and p_x^l and p_y^l (\cancel{p}_x^l and \cancel{p}_y^l) are the magnitude of the x and y components of the lepton's momentum (missing transverse energy), respectively.
- [34] J. Pumplin, D. R. Stump, J. Huston, H. L. Lai, P. Nadolsky, and W. K. Tung, J. High Energy Phys. **07**, 012 (2002).
- [35] T. Gleisberg *et al.*, J. High Energy Phys. **02**, 007 (2009). We use SHERPA version v1.4.
- [36] S. Catani *et al.*, J. High Energy Phys. **11**, 063 (2001).
- [37] R. Brun *et al.*, GEANT3, Technical Report CERN-DD/EE/84-1, CERN, 1987.
- [38] R. Hamberg, W.L. van Neerven, and T. Matsuura, Nucl. Phys. B **359**, 343 (1991)[Erratum Nucl. Phys. B **644**, 403 (2002)].
- [39] V. M. Abazov *et al.* (D0 Collaboration), Phys. Lett. B **669**, 278 (2008).
- [40] V. M. Abazov *et al.* (D0 Collaboration), Phys. Lett. B **705**, 200 (2011).
- [41] S. Moch and P. Uwer, Phys. Rev. D **78** 034003 (2008).
- [42] N. Kidonakis, Phys. Rev. D **74** 114012 (2006).
- [43] J. Campell, R. K. Ellis, Nucl. Phys. Proc. Suppl. **205-206**, 10 (2010). Version 6.1 is used.
- [44] V. M. Abazov *et al.* (D0 Collaboration), Nucl. Instrum. Methods A **763**, 290 (2014).
- [45] V. M. Abazov *et al.* (D0 Collaboration), Phys. Rev. D **83**, 031105 (2011).
- [46] V. M. Abazov *et al.* (D0 Collaboration), Phys. Lett. B **714**,32 (2012).
- [47] V. M. Abazov *et al.* (D0 Collaboration), Phys. Lett. B **719**, 354 (2013).
- [48] T. Andeen *et al.*, FERMILAB-TM-2365 (2007).
- [49] G. D. Lafferty and T. R. Wyatt, Nucl. Instrum. Methods in Phys. Res. A **355**, 541 (1995).
- [50] A. D. Martin, W. J. Stirling, R. S. Thorne, and G. Watt, Eur. Phys. J. C **63**, 189 (2009).
- [51] H. L. Lai, *et al.*, Phys. Rev. D **82**, 074024 (2010).
- [52] C. Amsler, Phys. Lett. B **667**, 1 (2008); see Section 17.8.
- [53] R. Aaij *et al.* (LHCb Collaboration), J. High Energy Phys. **06**, 141 (2012).
- [54] G. Aad *et al.* (ATLAS Collaboration), Phys. Rev. D **85**, 052005 (2012).
- [55] V. M. Abazov *et al.* (D0 Collaboration), Phys. Rev. Lett. **112**, 042001 (2014).
- [56] A. Kayis-Topaksu *et al.* (CHORUS Collaboration), New J.Phys. **13**, 093002 (2011).
- [57] S. Alekhin *et al.*, arXiv:1404.6469 [hep-ph].